Advanced Materials Interfaces

www.advmatinterfaces.de

Research Article OPEN ACCESS

Opportunities for Multiscale Pattern Modulation with Temporally Arrested Breath Figures

Francis J. Dent[1] | Maximilian Dreisbach[2] | Jochen Kriegseis[2] | Alexander Stroh[2] | Hiroshi Yabu[3] | Sepideh Khodaparast[1]

[1]School of Mechanical Engineering, University of Leeds, UK | [2]Institute of Fluid Mechanics (ISTM), Karlsruhe Institute of Technology (KIT), Germany | [3]Advanced Institute for Materials Research (WPI-AIMR), Tohoku University, Japan

Correspondence: Francis J. Dent (f.j.dent@leeds.ac.uk) | Sepideh Khodaparast (s.khodaparast@leeds.ac.uk)

Received: 4 September 2025 | **Revised:** 13 November 2025 | **Accepted:** 17 November 2025

Keywords: breath figure | condensation | membrane fabrication | micropatterning | porous films | self-assembly

ABSTRACT

Fluid-mediated patterning techniques offer a promising avenue for the cost-effective and scalable fabrication of structured surfaces across multiple length scales. Widespread adoption of fluid-based approaches, however, requires an in-depth understanding of the governing mechanisms to ensure precise control over pattern formation and dynamics toward reliable and affordable design modulation. Here, we present control strategies for creating diverse surface architectures by employing condensate water droplets as dynamic microscale templates. The temporally arrested breath figure patterning technique used here provides the opportunity for macroscale pattern organization with an elevated level of structural modification. We demonstrate systematic variation over isotropic and directional anisotropic breath figure micropatterns, leveraging control over the governing thermodynamic and photochemical phase change processes. Finely-tuned pattern formation is achieved in an order of minutes, creating breath figures of droplets ranging in size from hundreds of nanometers to tens of microns. Potential modulated surface architectures include organized macroscale spatial arrangements of breath figure pores, through-pore perforated membranes of discrete sizes, and elastomeric replication to transform the re-entrant cavity designs into protruding spherical caps. This adapted breath figure patterning technique thus provides a fast, scalable, and low-cost method for fabricating tunable surface morphologies tailored for future functionality.

1 | Introduction

Surfaces represent the boundaries for solid materials, largely defining the interactions between objects and their surrounding environment through various physical, chemical and biological exchange [1]. The nano and microstructuring of surfaces with features of length scales commensurate with natural entities (e.g. photonic wavelengths, biomolecules, microdroplets) unlocks new properties beyond those of the bulk materials, enabling novel emerging technologies. Large-scale surface patterning of nano and microscale features, however, is inherently challenging due to the antagonistic scales in manufacturing small features over large areas. Further, common microfabrication techniques based on lithographic or precision machining are expensive and scale-limited; long lead times with low throughput, multi-step processes coupled with requirements for clean-room facilities and specialized materials limit their functionality [2]. Practical use of such patterned surfaces is hence contingent on the ease of processing and manufacturing, with particular consideration for the simplicity, scalability, adaptability and associated costs.

More recently, bottom-up self-assembling approaches have received interest because of the ability to readily create small and complex features in a scalable and low-cost manner [3–5].

---

https://doi.org/10.1002/admi.202500811

Bottom-up approaches involve the creation of a pattern from the assembly of constituent elements, typically harnessing the growth of material, aggregation or self-assembling of particles [6]. Due to the favorable down-scaling in length at the target feature size, exploiting interfacial effects and instabilities facilitates the spontaneous creation or assembly of intricate features over large areas [7]. In particular, fluid-mediated strategies offer a host of potential patterning methods with varying degrees of resolution, accuracy and control [5]. This can range from molecular scales, at which phase separation methods facilitate self-assembly due to miscibility and de-mixing [8, 9], to larger-scale colloidal particle patterning [4, 7]. Techniques can be used in isolation, creating features with varying degrees of control and order, or further used to complement existing approaches, creating low-cost masks for lithographical methods or as secondary length scales on existing features [10, 11]. The ability to reliably create controlled nano-microscale surface features at both low cost and application-rational length scales is critical to the exploitation and wide-scale adoption of fluid-mediated manufacturing.

This paper looks more in-depth at the breath figure (BF) patterning methodology, valued for its inherent simplicity and accessibility [12]. In the BF approach, condensate droplets from a humid environment act as dynamic templates to pattern a polymer solution [13, 14]; heterogeneously nucleated droplets stabilize at the air-polymer interface and grow in size, self-assembling before complete evaporation of the solvent. Subsequent evaporation of the droplets reveal the latent imprinted pattern. The scalability of the method arises from the dynamic template generated by spontaneously formed water droplets, which is limited only by the initial polymer solution surface area that can be formed under a humid atmosphere. Drawbacks, however, typically stem from the limited ability to systematically vary the pattern characteristics due to the empirical control handles and the largely passive nature of the classical technique. The capability of imparting new material functionality through topographical surface modification for different applications is not only contingent upon low-cost and scalable methods, but on the ability to create controllable and variable features. As such, this paper summarizes the BF technique, along with its advantages and shortcomings, and briefly introduces various developed adaptations. Within this context, opportunities for design modulation in the temporally arrested BF methodology [15] are highlighted, building upon our previously reported mechanistic understandings of the underlying condensation dynamics.

2 | Breath Figure Patterning

The original BF patterning approach was developed in the 1990s when highly ordered, hexagonally packed porous surfaces were created by casting solutions of branched polymers dissolved in volatile solvents under humid conditions (Figure 1a) [13]. A low concentration of polymer (often < 10 wt%) is dissolved in a volatile organic solvent and drop cast onto a substrate [13, 14]. Under the right humidity conditions (typically 50% ≤ Relative Humidity (RH) ≤ 90%), evaporative cooling reduces the surface temperature of the polymeric solution to below that of the system dew point (Figure 1a,i). With continued cooling from solvent evaporation, heterogeneous drop-wise condensation occurs on the upper boundary and imprints into the interface as a result of the balance of interfacial tensions. Droplets stabilize and grow at the polymer interface, self-organizing into a quasi-crystalline hexagonal array, characteristic of the BF honeycomb pattern (Figure 1a,ii). As the solvent completely evaporates, the polymer solidifies and the temperature rises back to the ambient condition; the imprinted droplet morphology is revealed upon droplet evaporation from the solidified film, with successful patterning creating a monodisperse, closely packed array of pores (Figure 1a,iii) [16].

Since the inception of the method, numerous mechanistic theories and adapted techniques have been developed and well summarized across notable reviews [12, 16, 17]. From herein, we thus refer to the classical technique as any approach that uses solvent evaporation from a dissolved polymer solution to drive the interfacial cooling and subsequent patterning. The majority of adapted BF strategies have stemmed from particular application-derived perspectives, involving the use of different polymer materials and substrates to enhance the versatility of the method [18–23]. Patterned surfaces have been created with particular engineering polymers for specific qualities, such as stimuli-responsive polymers [24, 25], fluorinated low surface energy polymers [26, 27] and photocurable polymers [28–31]. Similar studies have shown how recycled and sustainable materials such as cellulose [32] can be used, as well as sinterable ceramic precursors [33]. Alternative methods have also facilitated BF patterns on electrospun fibres [34], 3D substrates and confined geometries [35], as well as on liquid substrates producing completely porous and perforated geometries [36]. In particular, selective patterning methods have shown useful premise for the well-controlled spatial development of interfacial morphologies through the direct application of solvent to solid polymeric substrates [37, 38].

As a patterning approach, the ability to readily modulate the feature size is imperative for each specific application; pore size variation in BF has been used to create selective particle filters [39, 40], tune the adhesion in wetting scenarios [41], and create anti-reflective coatings [42]. Because the BF technique is governed by phase change phenomena, altering the system thermodynamics varies the output pattern [43]. The average pore size is commonly changed by varying the relative humidity (RH) or airflow of the system, changing the rate of condensation and thus growth of the templating droplets prior to complete evaporation of the solvent [17]. However, for a given polymer/solvent solution, only a narrow range of working RH results in a homogeneous pattern output, with the corresponding feature size being empirically derived. Overall, BF formation is the result of a highly non-equilibrium process with a continual temperature change and an increase in the polymer concentration over time. Additional complexity arises from the coupled effects of solvent evaporation on the formation and growth of the condensate droplets, as well as the arrest and solidification of the final pattern [44]. Due to the overall temperature drop being a result of the evaporation of the finite solvent volume in this classical method, altering the environmental RH outside of a strict range may result in no visible pores occurring (too little condensation), or the contrary, with multilayer or irregular pores in the final pattern (too much condensation). As the solution temperature needs to drop below that of the dew point, the type of input polymer/solvent and

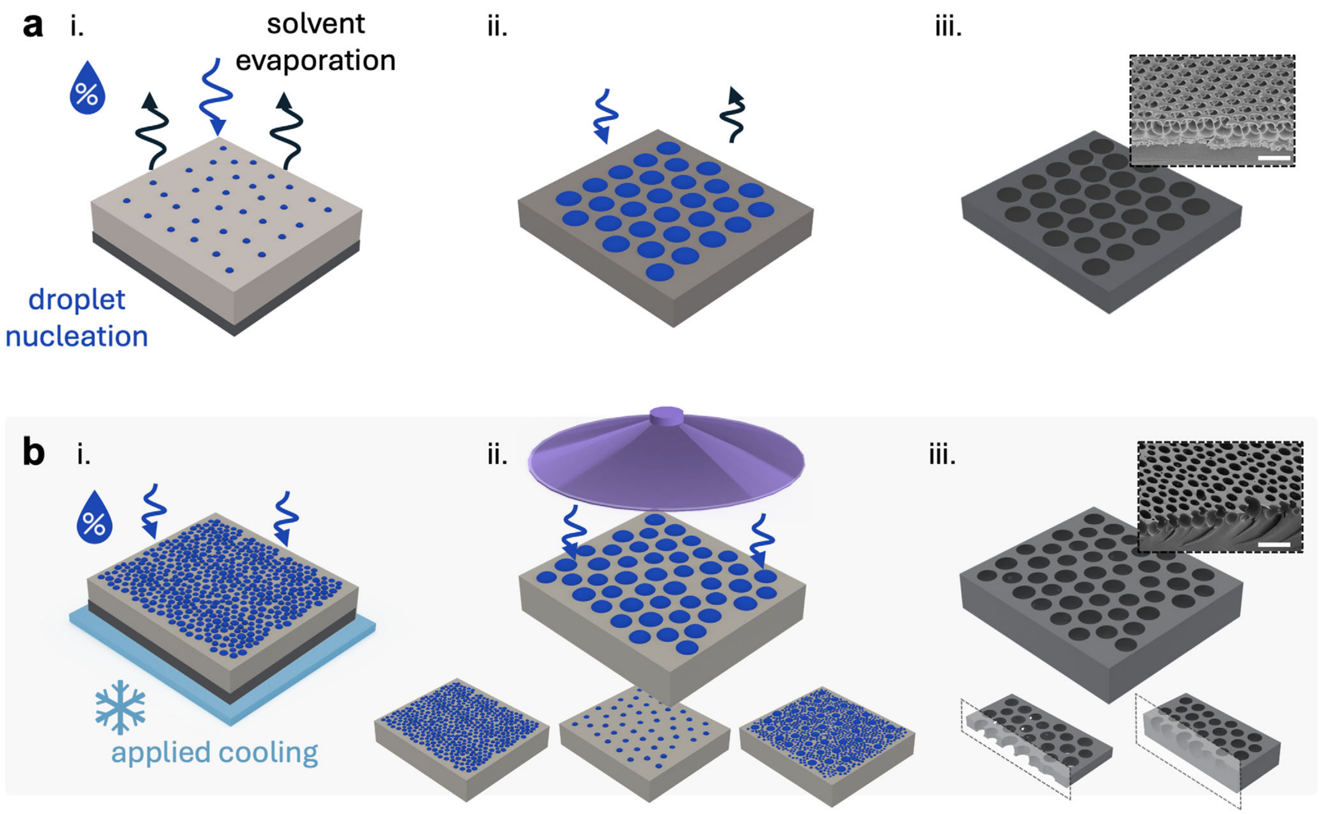

FIGURE 1 | Schematic illustration of (a) classical solvent-evaporation vs. (b) temporally arrested breath figure patterning pathways. In both methods, (i) drop-wise condensation occurs at the air-polymer interface and (ii) droplets continue to grow and self-assemble. (iii) Complete solidification of the polymer film and evaporation of the templating droplet array results in the generation of a porous pattern. Upper crops in both (a) and (b) show SEM images of patterned samples; the scale bar corresponds to 20 μm. Schematic insets in (b) demonstrate the pattern modulation potential via the temporally arrested technique.

relative concentrations can be somewhat varied to change the output pattern, however an effective feasible pattern window limits the ability to systematically vary the pattern characteristics [45]. Altering these parameters strikes a balance between adequately stabilized droplets and sufficient self-assembly from convection and thermocapillary forces to order the resultant pattern [46]. Ultimately, for a suitable polymer/solvent combination, the problem of creating effective and systematically varied patterns is governed in the temporal domain by the system thermodynamics.

While the coupled effects in classical BF make the passive technique uniquely powerful and adaptable for creating ordered patterned films from minimal intervention, the competing mechanisms limit the ability to readily control and systematically vary the resultant pattern. The deterministic design of the BF output requires critical control over all stages of the phase changes involved in the process, including initial condensation nucleation, kinetics of droplet growth, and final solidification of the solution. In classical BF, solvent evaporation drives the nucleation of condensation droplets. This leads to ambiguity around solvent compatibility - studies often have conflicting results because of the specific environmental conditions in their experiments [45]. Depending on the ambient or set humidity, evaporation of the solvents in question may or may not yield the required energy removal to produce sufficient cooling for the nucleation of the droplets. Enhanced or restricted thermal conduction through the substrate underneath the film introduces further complications in determining the subcooling level on the polymer film [45]. Consequently, prediction and control of condensation nucleation and subsequent pattern growth in the solvent-driven BF approach are challenging, if not impossible, due to the complex temperature variation over the duration of the experimental working time [47].

Variation in BF pattern size is classically attained through environmental control of temperature/humidity and the variation of the input parameters (e.g. polymer/solvent ratio) to modulate the duration of dynamic condensation [45]. By altering these input conditions, the feature sizes can be somewhat modulated, however, this has combined effects on the pore morphology and sinking depth due to the variation of interfacial tension and viscosity with time, with no direct control over the evolving film thickness [48]. Overall, the unpredictable spatio-temporal variation of thermodynamic conditions is incompatible with the drive to control and predict the resultant pattern size a priori. Only after complete solvent evaporation in the classical approach does one attain knowledge of the pattern feature size. This translates to an empirically-derived workflow that for every parameter/variable combination, a single final pattern is achieved. Much of the BF literature regards studies of this variation, with successful (monodisperse) or unsuccessful (semi-coalesced or incomplete coverage) patterning conclusions for variable input conditions [46].

3 | Temporally Arrested Breath Figure

In a recent development, we achieved direct in situ control over the size and distribution of the microscale BF patterns through complete decoupling of the cooling-driven condensation and film solidification processes (Figure 1b). The so-called temporally arrested breath figure approach [15] employs active cooling of the polymer using a Peltier device to finely tune the thermodynamic subcooling level (Figure 1b,i), facilitating novel droplet pattern morphologies illustrated schematically in the inset in Figure 1b,ii. In situ visualization of the pattern dynamics reveals well-described linear condensation growth dynamics for systems with large initial nucleation densities from early stages of the process. By using a UV curable polymer and no solvent, the predictable BF pattern on the liquid film can be instantaneously cross-linked to arrest the pattern growth Figure 1b,ii [15]. Patterned surfaces or porous membranes of specific feature sizes are achieved, depending on the initial film thickness and the time at which UV curing is completed Figure 1b,iii. As a result, the pattern evolution is directly and systematically influenced in the temporal domain, facilitating better control and application of the condensation physics [49].

In this adapted approach, external cooling facilitated by a Peltier device situated below the polymer film enables regulation of the supersaturation level and thus control over condensation nucleation and growth. The subcooling level of the polymer film can hence be set by measuring the dew point of the environment and setting the respective temperature difference. This is simplified from the classical approach whereby simultaneous and non-linear processes of solvent evaporation and water condensation occur, contrary to the controlled condensation dynamics in the temporally arrested approach prior to arrest, see arrows in Figure 1a,b. We have reported effective control over the size [15] and spacing [49] of the condensate droplet physics in the liquid state based on solutions for the temporally arrested breath figure technique, see Figure 1b,ii insets. Actively setting the level of supersaturation through the substrate temperature facilitates a direct correlation between the environmental conditions and predictable condensation physics. The ability to arrest pattern growth at discrete times through UV irradiation further enables the opportunity to translate the desired liquid pattern characteristics into a solid sample for varying applications [50].

The combination of control handles provided by the temporally arrested BF approach not only facilitates prediction and control over the droplet growth rates, but provides additional opportunities for the realization of unconventional breath figure patterns and the translation of these droplet manipulations into porous structured features. While we have previously reported upon in situ studies for the control of condensate droplets, the ultimate capability for the creation of diverse solid patterns has not yet been fully highlighted. Here, we briefly review the translation of controlled breath figure droplet pattern dynamics to solid structured surfaces with pores of different sizes and spacing. Building upon these capabilities, we demonstrate the fabrication of novel patterns with directional gradients through exploitation of a series of thermal and photocuring controls. Both in situ manipulation of the templating droplets and their respective patterns, as well as ex situ transformation of the patterned films, are outlined. We demonstrate a wide range of morphological architectures, including interfacial and through-porous membranes, and outward-protruding features.

3.1 | In Situ Modulation

3.1.1 | Isotropic Variation

The temporally arrested breath figure method relies upon the nucleation and growth of quasi-stable droplets at an air-polymer interface to template the polymer film prior to solidification. Quiescent environmental conditions are established by setting the specific subcooling level using a Peltier cooling device, leading to observations of well-defined condensation growth laws [43]. NOA63 photocurable polymer is used as the model material for the thin film due to its fast and oxygen-tolerant cross-linking, as well as facilitating a high nucleation density of droplets [15]. As shown in the experimental setup and in situ analysis in Figure 2a,b, when droplets have reached the desired feature size after a period of minutes, a short flash of UV irradiation arrests the growth kinetics of the droplets by cross-linking the polymer film. Upon returning the Peltier temperature to that of the ambient laboratory, the water droplets evaporate, revealing the latent pore imprint as shown in the SEM images of Figure 2c.

At a constant subcooling level, droplets at the air-polymer interface grow in close contact with neighboring droplets due to the high nucleation density exhibited on NOA63. Figure 2b inset images show in situ droplet growth snapshots at discrete times where growth can be arrested to create patterns ranging in average feature size, D_s, from 100's nm to 10's µm. Due to the highly packed nature of the pattern, droplets are quasi-stable and only coalesce after the eventual draining of the viscous polymer bridge between neighboring droplets, resulting in the overall increase in feature size [15]. We have previously quantified the liquid droplet growth physics in this system whereby the average droplet size increases linearly with time due to macro coalescence effects. This well-described law is obtained from the combined effect of growth through diffusion and the direct accumulation of water molecules on the droplet surface, as well as the effect of significant coalescence between neighboring droplets [43, 51]. Due to the 3D growth of droplets measured in terms of diameter, the area fraction of a coalesced droplet is less than the sum of the original droplets, resulting in a self-similar growth regime. A constant area fraction of droplet coverage is observed throughout the pattern evolution, regardless of droplet size, with a low polydispersity of 15 ± 5% in droplet size [15].

By experimenting with the subcooling temperature in the range of 5°C–10°C below the dew point, average experimental working times for droplets to nucleate and grow into micro sized features prior to curing and pattern arrest are on the order of minutes. There is a direct translation of the condensate droplet growth kinetics to the cured pattern. The quasi-instantaneous cross-linking has a negligible effect on the transition from templating liquid droplets to the solid templated imprint (BF pore). Using real-time analysis of growing droplets in the liquid state, the transient curing process can hence be scheduled to create features of specific sizes. With a constant subcooling temperature applied, as

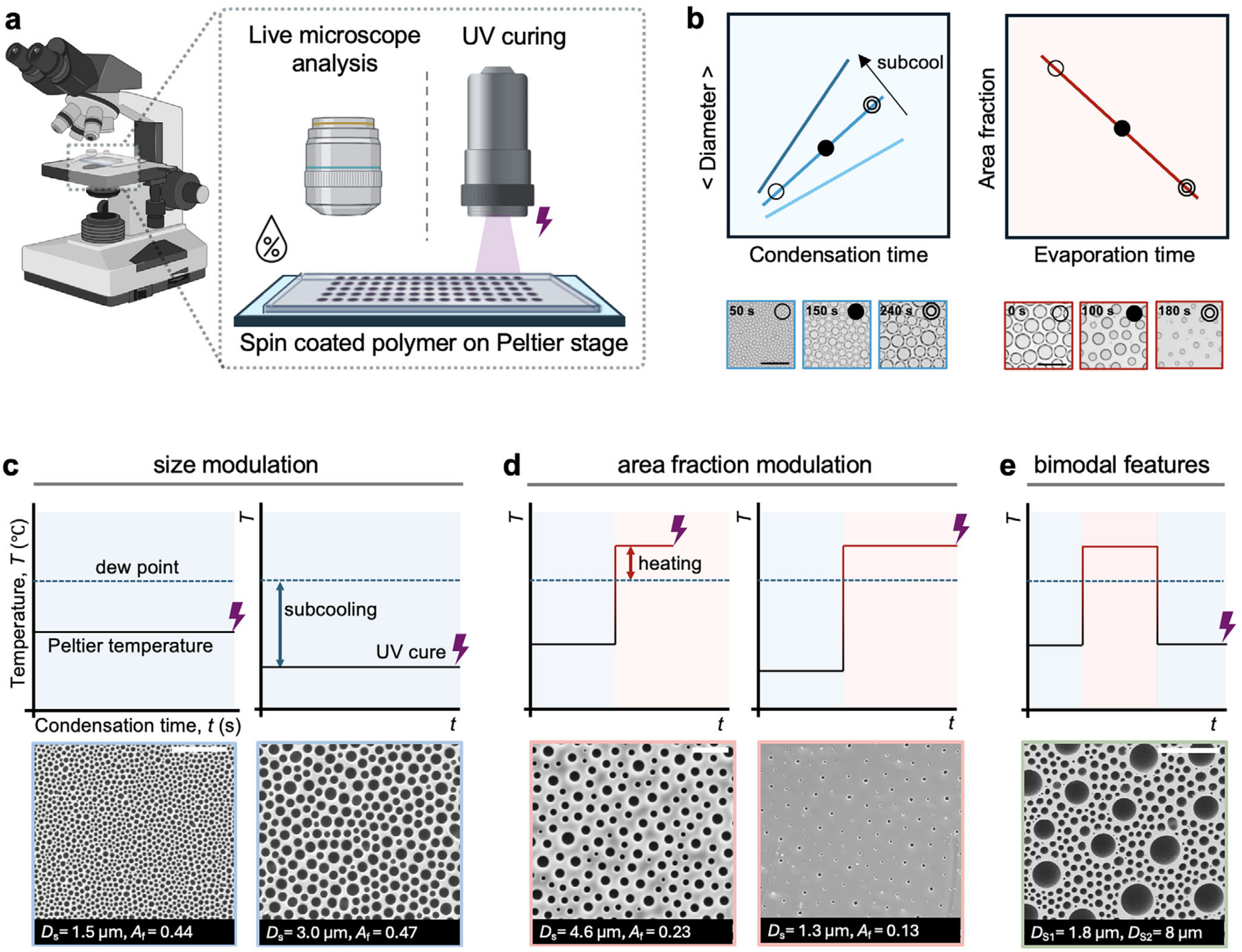

FIGURE 2 | (a) Schematic illustration of the experimental set-up. (b) In situ analysis of droplets in the liquid state prior to cross-linking of the polymer film and pattern arrest. (c) Average diameter grows linearly in time at constant subcooling, with droplet growth rate proportional to the set subcool. (d) Heating of an established droplet pattern results in droplet evaporation and a decreased packing density in the final cured pattern. (e) A final subcooling phase can restart condensation on the free surface area resulting in a bimodal distribution. Inset images in (b) show the droplet pattern evolution with optical microscopy, compared to SEM images in (c)–(e) demonstrating the cured porous patterns after UV irradiation. All scale bars correspond to 20 μm.

droplets interact and coalesce, the average droplet size increases linearly with condensation working time. This regime hence controls the average feature size for highly packed conditions, where the area fraction (A_f) of surface covered by pores remains constant at approximately $A_f = 0.45 \pm 0.05$ (Figure 2c). While droplets grow linearly in time in this growth regime, the subcool level dictates the growth rate; Figure 2c shows samples created by UV curing after 150 s of subcooling at $\Delta T_C = 5$°C and $\Delta T_C =$ 10°C, respectively. Both temperature and condensation working time can hence be altered to change the final average feature size.

Area fraction modulation can be programmed in situ by heating the established BF patterns of liquid droplets to temperatures above the dew point. As the size of droplets is controlled by the thermodynamic state of the system, a pattern of specific droplet size and area fraction can be subsequently modulated through Peltier heating, thereby initiating evaporation of the droplets. (Figure 2d). Due to the high viscosity of the polymer (2 Pa.s) and subsurface droplet morphology exhibiting minimal meniscus, capillary interactions are insignificant. Upon evaporation, droplets shrink radially in time without observable attraction to one another, conserving the interdroplet spacing distance and inducing a decrease in the area fraction coverage. The evaporation kinetics of droplets follow previously observed laws [49], where individual droplets initially evaporate at a rate $D^2 \propto t$ with the area fraction decreasing linearly over time (Figure 2b). The spacing between droplets and features is therefore determined by the initial cooling regime as droplets grow in the highly packed state, after which the droplets shrink with heating to the desired feature size/area fraction at which point the pattern evolution is arrested through UV exposure. Inset images in Figure 2b (right) shows the area fraction analysis of the evaporating liquid droplets, where modulation occurs at a constant interdroplet spacing; cured pattern examples of modulated area fraction are shown in Figure 2d. Due to thermal effects resulting in eventual droplet sinking and non-linear growth [49], low heating above the dew point ($\Delta T_H = 1 - 5\,$°C) is done to steadily decrease the surface coverage without completely evaporating the droplet array or creating strong internal flows to ensure strict feature control.

The ability to modulate the pattern characteristics can be further explored by combining repeated cycles of droplet growth (subcooling) and shrinkage (heating). As an initial example, bimodal patterns or patterns with hierarchical size domains are fabricated by restarting the condensation process on spatially modulated samples in the liquid state. By having a second subcooling step following an evaporation regime, new families of droplets nucleate on the free space between the pre-existing droplets (Figure 2e). Like before, the initial cooling stage of highly packed droplets determines the interdroplet spacing, which remains constant during the heating phase. The heating phase determines the extent of spatial modulation by evaporating the droplets, resulting in a decrease in droplet area fraction. It is this free surface area where new droplet families nucleate during the subcooling - a large temperature difference is required for the second cooling phase to initiate a high nucleation density of new droplets. The existing large droplets continue to grow at the constant interdroplet spacing, acting as humidity sinks within their immediate vicinity. Constant image analysis feedback is hence required to trace the point at which the new droplets are densely packed enough at the required size to arrest the growth through UV curing. The option to create both spatially modulated and bimodal patterns is not conventionally accessible via self-assembling methods alone, which rely upon capillary interactions to assemble.

While limits to this in situ control exist, we readily demonstrate cured patterns of highly packed features from 100's nm to 10's µm, synonymous with the scale of natural functional surface features. Due to the method being governed by thermodynamic state, this temporally arrested technique provides greater control over the growth rate by setting the level of supersaturation through external cooling on the Peltier device, rather than relying on the concentration and type of solvent used. Droplet coalescence exhibiting a small and consistent polydispersity in feature size (10–15%) is accepted as a compromise over highly ordered features that are less controlled in size with the classical BF method.

3.1.2 | Anisotropic Variation

Thermodynamic Control As thermodynamic control over the set temperature and environmental dew point can alter the BF pattern isotropically, varying the substrate temperature spatially can engender variable condensation growth rates to exploit anisotropic designs over larger scales. The ability to create macroscale gradients in topography opens up new potential applications for fabricated patterned films and further demonstrates the versatility of the fabrication approach, beyond what is classically attainable through self-assembly techniques. The evidenced control over pattern evolution on NOA63 due to substrate temperature control, combined with the use of photocurable polymers, thus facilitates new capabilities to create macroscale variation over the microscale features, as illustrated in Figure 3.

Due to the high droplet nucleation density exhibited on NOA63, for a set subcooling level, we see that the average feature diameter grows linearly in time at a rate proportional to the subcool level, producing patterns with a near-constant packing over the cooled area [49]. As such, temperature gradients across the substrate can be implemented to take advantage of the variable droplet growth rate. Depending on the spatially applied temperature, the growth of the BF droplets and resultant pattern can be both discontinuous and continuous (Figure 3a). In an area with a constant subcool, the pattern results in a constant droplet size. As the level of subcooling decreases, droplets grow at a slower rate, resulting in a gradient. The overall droplet pattern can then be translated into a cured design by cross-linking the full sample as before. We can hence ascribe a pattern gradient α to the inverse of the change in average feature diameter ΔD divided by the characteristic length L over which the pattern varies, $\alpha = \left(\frac{\Delta D}{L}\right)^{-1}$. Smaller and larger α hence correspond to more abrupt or smoother pattern variation, respectively (Figure 3a).

Figure 3b shows the schematically applied cooling with inset images indicating the actual infrared temperature measurements on the cooled cover slips; lower and higher temperatures appear in blue and pink, respectively, alongside macro images of the fabricated patterned cover slips, and SEM close-ups of the patterned regions. As before, when a constant subcooling is applied, the BF pattern is isotropic over the full temperature-controlled region, resulting in a homogeneous pattern (Figure 3b,i). The strictest gradient, exhibiting a switch from pattern to no pattern over the course of a relatively sharp boundary (10's µm) can be created by only partially exposing the sample to the subcooled Peltier stage. The section of the film held at temperatures below the dew point will develop BF patterns while the rest of the film at the ambient temperature remains unchanged (Figure 3b,ii). This results in α values on the order of 10's, where the sharp transition occurs over a minimal distance comparable to that of the feature size. A more diffuse gradient of BF pattern size ($\alpha = \mathcal{O}(10^3 - 10^4)$) can be generated by placing the polymer film on a thermally conductive substrate with the two ends held at temperatures below and above the dew point. This configuration yields a gradual, continuous boundary between the patterned and non-patterned section, whose width depends on the imposed lateral temperature gradient and thermal conductivity of the substrate. Figure 3b,iii shows an example of the diffuse transition between BF patterns with an average pore diameter varying by an order of magnitude between 3 and 0.4 µm. Variations of more complex macroscale patterns can hence be created by spatially altering the substrate temperature prior to the arrest of the droplet growth. For example, Figure 3c shows the resulting patterns obtained by exposing the polymeric film to a flat subcooled metallic grid with circular (left) and square (right) apertures, which translate to subcooled and non-subcooled regions. More optimized thermal masks can be created that allow for good airflow to the non-cooled regions to ensure there is minimal unintended cooling; if cool air is trapped, a larger α gradient arises as droplet nucleation and growth occurs at any region that is below the temperature of the dew point.

Photomasking In classical BF, photosensitive polymers have been used to create strong cross-linked films or to functionalize patterns, often post fabrication [25, 31, 52, 53]. Due to the evaporation-driven formation mechanism in the classical technique, photomasks have mostly been used ex situ for creating

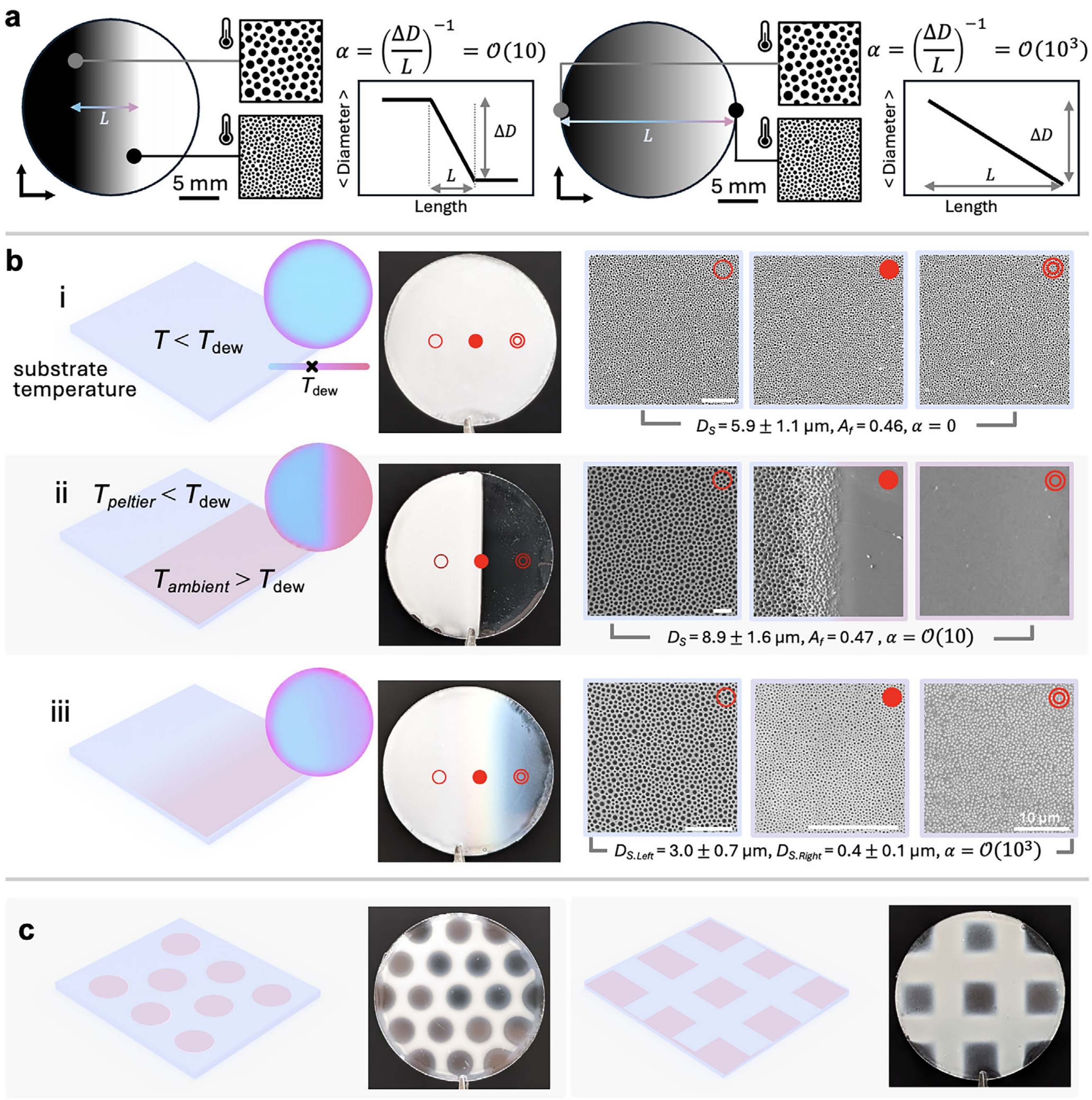

FIGURE 3 | Anisotropic pattern variation capability enabled by substrate temperature control. (a) Schematic representation of discontinuous and continuous gradient variation. (b) From left to right, panels show a schematic of the applied cooling temperature with inset infrared measurements on the round cover slip (indicated color range from 4°C, blue - 24°C, red), images of cured patterns on cover slips and SEM crops of respective patterns; (i) homogeneous cooling produces an isotropic pattern, (ii) binary pattern to no-pattern transition created by cooling half of the polymer film, (iii) gradient pattern from the diffuse temperature gradient on substrate, creating variation in feature size from micro to nanoscale (left to right). (c) Variations of subcooling masks imposing circular and square grid designs. SEM scale bar corresponds to 40 µm unless otherwise stated.

spatially varied patterns, exposing complete patterned films to UV irradiation to post-modify the structure [31, 53]. In contrast, temporally arrested BF uses polymers which can be selectively irradiated in situ as well as at discrete time points to spatially arrest pattern areas of different feature sizes.

In a similar manner to the thermal masking applied beneath the patterning film to implement spatial variation in features, the UV exposure can be varied from above to control the film solidification and subsequent pattern formation by spatially arresting the pattern growth (Figure 4). As the short UV exposure effectively arrests the droplet pattern and translates the observable liquid droplets into cured porous features, spatially controlling the UV exposure through UV opaque photomasks provides another control handle to modulate the BF pattern over larger scales. For the current proof-of-concept analysis, UV opaque photomasks were used to selectively cure sections of the NOA63 films at discrete times. Masks were placed on top of the cooled polymeric

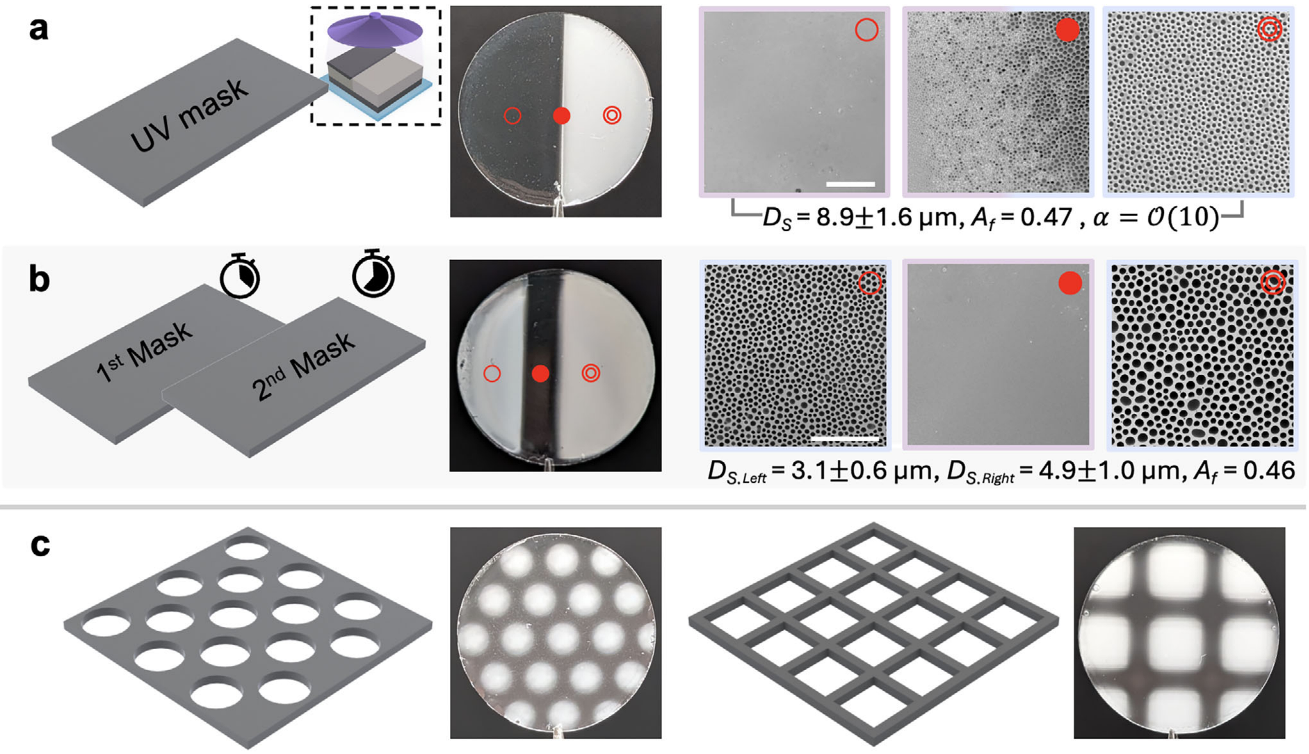

FIGURE 4 | Schematic of photomask set-up and corresponding patterned films. (a) Mask selectively controls the area exposed to UV, where (b) successive masks can also be used to create variable patterns and (c) circular and rectangular mesh masks to create more complex spatial patterns. Scale bars correspond to 50 µm.

film using a spacer to avoid direct contact and enable subsequent pattern modulations. Regions of BF patterned polymer that were exposed to the UV light through the transparent section immediately solidified, while droplet growth was maintained on the sections obstructed by the UV mask.

Spatially arrested patterns can be made with a two-step curing process; a droplet pattern is created before selectively exposing part of the substrate, arresting the droplet growth. The remaining liquid region with droplets can be evaporated before curing in order to obtain a smooth region (Figure 4a). Alternatively, secondary masking can be applied to introduce regions of newly developed patterns or solidify the original pattern after a longer period of time (Figure 4b). The same perforated masks from before in the thermal process were also applied above the film to selectively cure pattern areas, achieving the opposite spatial configurations, compare Figure 3d with Figure 4c.

3.2 | Ex situ Transformation

3.2.1 | Soft Replication

Soft replication of breath figure patterns enables the development of further diverse morphologies manifesting as protruding spherical caps. Replication of classical BF has been completed previously, where the BF material is commonly dissolved to enable release of the inverse shape due to the negative curvature of the BF pore (submerged droplet imprint) [54–57]. As classical patterns are often created in polystyrene and other brittle polymers, once the replica medium infiltrates and solidifies within the BF mold, the BF is destroyed, meaning every BF patterned sample can create a single replica.

The temporally arrested BF approach completed in cross-linked polymer films makes it possible to transform the porous structure into protruding caps without causing permanent damage to the original mold, as illustrated in Figure 5a. A commercial polydimethylsiloxane (PDMS) and cross-linker (Sylgard 184, Dow Corning) was used due to its mechanical properties, low surface energy and availability [58], enabling high fidelity replication of features and facile removal from the enclosed curvature of the BF pattern. The base and hardener were mixed at a 10:1 ratio and degassed for 30 min before the liquid polymer was poured over the respective BF and further degassed to remove entrapped air from the cavities. Successive replicas can thus be created for a singular BF pattern as the PDMS effectively detaches from the BF pattern, producing high fidelity replication of diverse architectures with varied pore size and distribution (Figure 5b), as well as designs with a directional pattern gradients (Figure 5c).

Secondary replication of the protruding pattern can also be completed to create an analogous BF porous pattern in a new material. Here, PDMS–PDMS replications are demonstrated to create both protruding and porous patterned films in the same materials to enable pattern comparison. Double replication was performed by plasma cleaning the first replica for 2 min prior to silanization in a desiccator with 250 µL of chlorotrimethylsilane (Sigma–Aldrich) for 2 h. The silanized PDMS replica is needed to ensure effective detachment of the second porous PDMS replication from the the first protruding replica made up of the same material (Figure 5a,ii/iii). PDMS soft lithography was

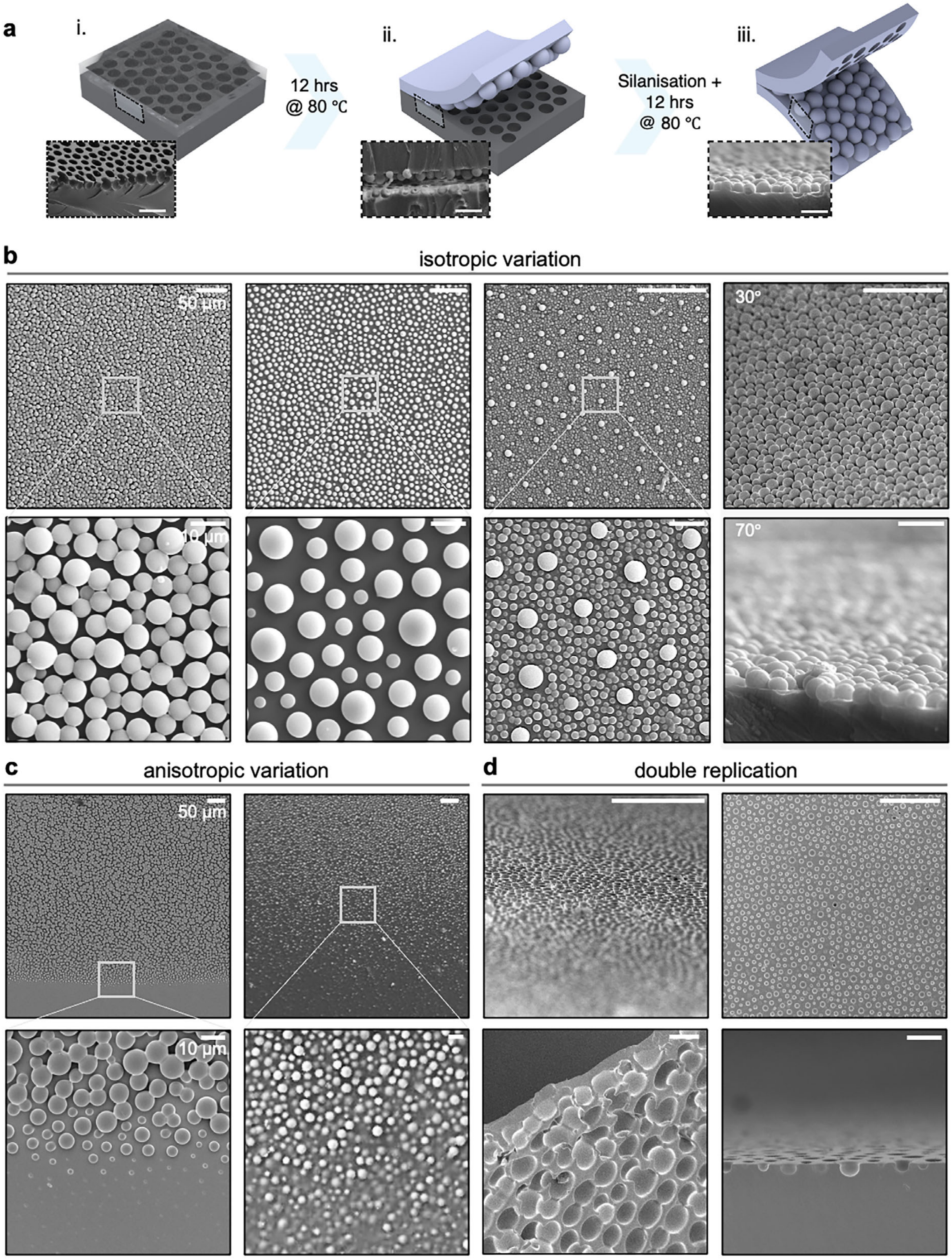

FIGURE 5 | Soft lithography of temporally arrested breath figure and corresponding protruding features. (a) Schematic illustration of replication process where (i) pre-mixed liquid PDMS is infiltrated into a breath figure pattern (SEM showing cross section of BF). (ii) After curing the PDMS overnight, the PDMS can be gently peeled from the BF sample. (iii) A secondary replication of the pattern can be created to re-create the porous BF morphology in PDMS medium. SEM top view and inclined images of (b) protruding replica samples generated from isotropic BF patterns, (c) anisotropic surfaces and (d) secondary replication in PDMS (analogous BF features). Scale bars in (b), (c) and (d) correspond to 50 μm in the large area images, and 10 μm in magnified views.

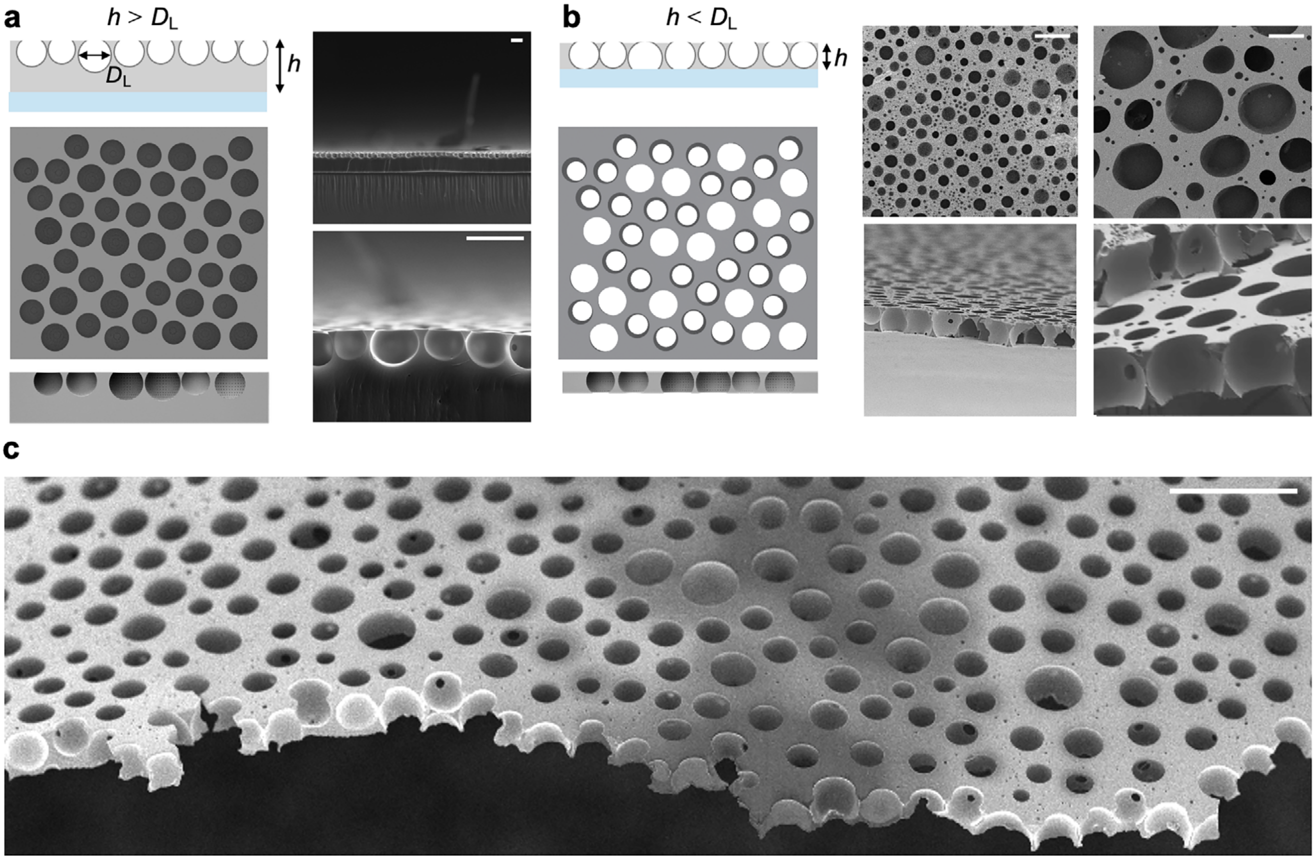

FIGURE 6 | Fabrication of breath figure patterns and membrane formation. By spin coating for a longer duration or making a thinner polymer film, templating droplets can contact the substrate and create through-pore geometry. (a) Standard pattern formation where the thickness of the thin film is greater than the average droplet size compared to (b) films thinner than the average droplet creating small pore (≈5 µm, left) and large pore (≈25 µm, right) membranes. (c) SEM images showing the material flexibility and scalability of the membrane fabrication method for small pores. Scale bars correspond to 20 µm.

then completed on the silanized sample in the same manner as before. SEM images in Figure 5d show angled views of highly packed and spaced double-replicated samples to differentiate the morphology.

3.2.2 | Membrane Fabrication

Polymeric membranes and microseives have wide-ranging applications in areas from cell culturing and analysis, filtration and separation, to the production of emulsions [59, 60]. The ability to tune the membrane area and pore size (porosity density range) is essential for the different technological interests. Conventional techniques through track-etching and electrospinning make it difficult to control pore positioning and thus limit the overall control and accuracy of porosity. While breath figure techniques have been used to successfully create porous membranes [61–63], the inability to systematically vary the pore size, area coverage, and film thickness limits its adaptability.

By combining in situ modulation of the droplet size and ex situ transformation of film removal from the substrate, through-pore perforated membranes can be fabricated using the temporally arrested BF technique. To create the BF, the average liquid droplet diameter D_L has to be less than the initial film thickness h to ensure no substrate-droplet interactions (Figure 6a). When the dimensions of the droplet array are significantly smaller than that of the polymer film, there is little to no difference in the overall film thickness when accounting for material displacement. To create membrane porous films, the average droplet size needs to be commensurate to the film thickness. To ensure substrate-droplet interactions that create a through-pore, however, the film thickness has to be created to around 1/4 thickness of the target pore diameter. This constraint facilitates the increasing effect of polymer displacement as the droplet array volume becomes significant in relation to the film thickness. Due to the highly packed droplet array, accounting for an area coverage of around 75% below the film [15] because of the submerged droplet morphology (see liquid images in Figure 2b), an initial thinner film has to be produced to account for the displacement. For example, to create pores of approximately 10 µm, a spin coated film of around 2.5 µm is required to account for the displacement of polymer as the water droplet array grows to reach the desired dimensions. To further optimize the process, different supporting substrates with varying wetting and adhesion characteristics were tested to ensure the patterned film could be released and peeled from the substrate. Figure 6b demonstrates the film thickness relationship with SEM examples of small pores, approximately 5 µm (left), and larger pores of 25 µm (right).

As the average droplet diameter grows larger than the film thickness ($D_L > h$), substrate interactions become significant, and wetting effects between the polymer-droplet-substrate need to be taken into consideration. If the interfacial tension between the droplet and the substrate is too great relative to the polymer, droplets will wet the substrate, causing the polymer film to de-wet. Standard glass substrates worked sufficiently; while some droplets de-wet from the top air-polymer interface and form a sessile droplet at the substrate-polymer interface, the majority of pores remain throughout the thickness of the polymer. Note that particularly at larger pore sizes $D_L > 10$'s µm, secondary nucleation is observed at the top air-polymer surface, however, due to their smaller size, these superficial pores remain at the interface and do not affect the membrane functionality.

4 | Conclusions

Fluid-based fabrication methods enable the ability to readily pattern surfaces over large areas, facilitated by low input material cost and intrinsic self-assembling forces. In particular, the BF method is one of the most facile examples of such approaches, requiring condensating water droplets from humid air to act as the templating mechanism input, creating defined patterns within minutes. The temporally arrested technique builds upon the original BF method, substituting passive developments with well-defined control handles, increasing the ability to modulate the pattern characteristics. As a result, in situ control through external cooling and photocuring permits varying size, spacing, and configuration characteristics in the patterning. By controlling the experimental time and substrate temperature, patterns are created consisting of highly packed features from 100's nm to 10's µm. Spatial variations of packing densities ranging from 0.45 to 0.1 area fraction can be implemented, as well as permutations of these combined effects.

Further in situ control through spatial modulation of the substrate temperature or UV-arrested area allows the addition of secondary macroscale motifs and directional functionality to the original microscale BF structure. Ex situ transformation, including successful soft replication of the original porous BF structures, produces surfaces with inverse protruding spherical cap structures of varied shape, size, and distribution with anisotropic interfacial properties facilitating potential low-cost fabrication methods for tunable functional materials. Furthermore, knowledge of the final patterned film thickness in the solvent-free approach allows specific control over coating thickness and formation of through-pores and the fabrication of thin membranes with specific pore sizes for potential filtration and masking functionalities. While we have performed these experiments in the most simplistic setup of an open laboratory environment, we obtained promising results regarding process robustness and control. Ultimately, as the patterning is contingent upon strict control of environmental conditions and substrate temperature control, with the predictable droplet growth physics the process could become fully programmable using an enclosed controlled environment.

Limits to the temporally arrested technique, however, arise from the material input. The photocurable polymer needs to be rapidly cross-linkable, ensuring quick solidification to arrest the liquid growth dynamics into a solid pattern. The cross-linking also has to be tolerant to oxygen to enable curing in atmospheric conditions, limiting the number of appropriate polymers. A high initial droplet nucleation density is essential for achieving mechanistic control of patterns across the multiple scales shown here. Classical BF enables the creation of domains of monodisperse pores as droplets grow and self-assemble without significant coalescence prior to the solidification of the polymer solution. As the condensation droplets grow primarily via coalescence in the temporally arrested approach, greater control over pattern characteristics is garnered at the expense of strict monodispersity. A small polydispersity of features in the highly packed regime of around 15% is the tradeoff for consistent and predictable control over the final pattern dimensions. While the classical method is dependent on the size and wetting of the casting substrate and input conditions, this method uses a spin coated polymer film to modulate the film thickness. Overall, when compared to other self-assembly techniques, this method achieves superior control with minimal input parameters, facilitating a wide breadth of pattern configurations without altering the materials.

5 | Materials and Methods

5.1 | Materials

Substrate Photocurable polymers were coated on standard borosilicate glass cover slips of 22 mm diameter with a thickness of 0.15 ± 0.02 mm. These were cleaned prior to use by washing with isopropanol (IPA) and deionized (DI) water before being dried in the oven overnight at 80°C. The cover slips were chosen due to their low-cost availability and optical transparency, enabling both transmission and reflected light optical microscopy analysis. The relative thinness of the cover slips facilitated effective heat transfer from the external cooling device, whilst providing a rigid support to maintain a flat, thin polymer film.

Polymer Norland Optical Adhesive NOA63 (Norland Products Inc.) polymer was used due to its mechanical properties and adhesion to substrates. The photo-induced cross-linking mechanism exhibits rapid curing in ambient conditions, low material shrinkage, and high resistance to solvent, oxidative and UV degradation, making it an excellent candidate for functional thin-film coatings [64, 65]. NOA63 was chosen over other NOA polymers due to the high nucleation density of droplets observed at the interface when subcooled [15], enabling arrest of systematically variable feature sizes from nano to microscale.

5.2 | Experimental Set-Up

Constant NOA film thickness was achieved through modulation of the spin coating parameters. For BF patterns of features up to around 10 µm, a 30 µm of NOA63 was spin coated to ensure negligible interaction between the droplets and the substrate. Porous membranes were created by spin coating NOA63 to a thickness of less than 5 µm and growing droplets of larger diameter than this.

Patterns were created by cooling the polymer-coated cover slip on a Peltier device (Linkham PE120) held at a constant temperature T_P during each experiment, accurate to within ±0.5°C. Subcooling temperature was calculated based on the difference between the measured dew point and the set Peltier temperature, $\Delta T_C = T_{dp} - T_P$. Condensation dynamics were monitored using an Olympus BX53M optical microscope (OM) in reflective mode, equipped with a long working distance objective (Olympus LMPLFLN 50X) and a digital CMOS camera (Basler ace acA2040-90uc). The droplet pattern evolution was analyzed in real-time using a developed MATLAB code to identify droplet boundaries [49]; this detects and measures all the features in the frame to compute an average feature diameter D_s, and feature density calculated as the area fraction of pores to overall surface area, $A_f = \frac{[\sum_{i=1}^{n} \pi(D_s^2/4)]}{A}$. At the desired feature size, the droplet pattern was arrested with a 5 s burst of UV light using a flood curing system (Dymax Bluewave AX-550 Redicure) with 365 nm irradiation wavelength, operated at a max intensity output of 425 mW/cm^2. The Peltier device is switched off after pattern arrest to allow the sample to return to ambient temperature and subsequent complete evaporation of the templated droplets. A further 5 s of UV irradiation was applied to ensure the pore cavities were fully cross-linked. The fabricated samples were then baked at 130°C for 1 h to remove any residual and unreacted functional groups at the interface.

Acknowledgements

F.J.D. was funded through an EPSRC Doctoral Prize Fellowship (EP/W524372/1). The authors acknowledge the generous funding provided by the Leeds Institute for Fluid Dynamics (LIFD) to facilitate the knowledge transfer exchanges between the UK, Germany and Japan.

Conflicts of Interest

The authors declare no conflict of interest.

Data Availability Statement

The data that support the findings of this study are available from the corresponding author upon reasonable request.

References

1. W. Barthlott, M. Mail, B. Bhushan, and K. Koch, “Plant Surfaces: Structures and Functions for Biomimetic Innovations,” *Nano-Micro Letters* 9 (2017): 23.

2. J. A. Liddle and G. M. Gallatin, “Nanomanufacturing: A Perspective,” *ACS Nano* 10, no. 3 (2016): 2995–3014.

3. J. D. Halley and D. A. Winkler, “Consistent Concepts of Self-Organization and Self-Assembly,” *Complexity* 14, no. 2 (2008): 10–17.

4. O. D. Velev and S. Gupta, “Materials Fabricated by Micro- and Nanoparticle Assembly – the Challenging Path from Science to Engineering,” *Advanced Materials* 21, no. 19 (2009): 1897–1905.

5. P.-T. Brun, “Fluid-Mediated Fabrication of Complex Assemblies,” *JACS Au* 2, no. 11 (2022): 2417–2425.

6. G. M. Whitesides and B. Grzybowski, “Self-Assembly at All Scales,” *Science* 295 (2002): 2418–2421.

7. N. Vogel, M. Retsch, C.-A. Fustin, A. del Campo, and U. Jonas, “Advances in Colloidal Assembly: The Design of Structure and Hierarchy in Two and Three Dimensions,” *Chemical Reviews* 115, no. 13 (2015): 6265–6311.

8. J. Bang, U. Jeong, D. Y. Ryu, T. P. Russell, and C. J. Hawker, “Block Copolymer Nanolithography: Translation of Molecular Level Control to Nanoscale Patterns,” *Advanced Materials* 21 (2009): 4769–4792.

9. L. Xue, J. Zhang, and Y. Han, “Phase Separation Induced Ordered Patterns in Thin Polymer Blend Films,” *Progress in Polymer Science (Oxford)* 37 (2012): 564–594.

10. M. Rey, F. J. Wendisch, E. S. A. Goerlitzer, et al., “Anisotropic Silicon Nanowire Arrays Fabricated by Colloidal Lithography,” *Nanoscale Advances* 3 (2021): 3634–3642.

11. M. Michalska, S. K. Laney, T. Li, M. K. Tiwari, I. P. Parkin, and I. Papakonstantinou, “A Route to Engineered High Aspect-Ratio Silicon Nanostructures through Regenerative Secondary Mask Lithography,” *Nanoscale* 14 (2022): 1847–1854.

12. J. Rodríguez-hernández and E. Bormashenko, *Breath Figures: Mechanisms of Multi-Scale Patterning and Strategies for Fabrication and Applications of Microstructured Functional Porous Surfaces* (Springer, 2020).

13. G. Widawski, M. Rawiso, and B. François, “Self-Organized Honeycomb Morphology of Star-Polymer Polystyrene Films,” *Nature* 369 (1994): 387–389.

14. B. François, O. Pitois, and J. François, “Polymer Films with a Self-Organized Honeycomb Morphology,” *Advanced Materials* 7 (1995): 1041–1044.

15. F. J. Dent, D. Harbottle, N. J. Warren, and S. Khodaparast, “Temporally Arrested Breath Figure,” *ACS Applied Materials and Interfaces* 14 (2022): 27435–27443.

16. H. Yabu, “Fabrication of Honeycomb Films by the Breath Figure Technique and their Applications,” *Science and Technology of Advanced Materials* 19 (2018): 802–822.

17. A. Zhang, H. Bai, and L. Li, “Breath Figure: A Nature-Inspired Preparation Method for Ordered Porous fFlms,” *Chemical Reviews* 115 (2015): 9801-9868.

18. M. T. Calejo, T. Ilmarinen, H. Skottman, and M. Kellomäki, “Breath Figures in Tissue Engineering and Drug Delivery: State-of-the-Art and Future Perspectives,” *Acta Biomaterialia* 66 (2018): 44–66.

19. Y. Wang, W. Zhou, Q. Kang, et al., “Patterning Islandlike Mno2 Arrays by Breath-Figure Templates for Flexible Transparent Supercapacitors,” *ACS Applied Materials & Interfaces* 10, no. 32 (2018): 27001–27008.

20. X. Wu, T. Liu, S. Gao, S. Chen, and Q. Lu, “Single Polar Cell Trapping Based on the Breath Figure Method,” *ACS Omega* 4, no. 23 (2019): 20223–20229.

21. X. Zhang, B. Wang, L. Huang, et al., “Breath Figure–Derived Porous Semiconducting Films for Organic Electronics,” *Science Advances* 6, no. 13 (2020): eaaz1042.

22. C. Liu, M. Wu, L. Gao, H. Liu, and J. Yu, “Nanoporous Polymer Films Based on Breath Figure Method for Stretchable Chemiresistive No2 Gas Sensors,” *Sensors and Actuators B: Chemical* 371 (2022): 132540.

23. N. Salaris, P. Haigh, I. Papakonstantinou, and M. K. Tiwari, “Self-Assembled Porous Polymer Films for Improved Oxygen Sensing,” *Sensors and Actuators B: Chemical* 374 (2023): 132794.

24. S. Chen, S. Gao, J. Jing, and Q. Lu, “Designing 3D Biological Surfaces via the Breath-Figure Method,” *Advanced Healthcare Materials* 7 (2018): 1–18.

25. M. Kojima, T. Nakanishi, Y. Hirai, H. Yabu, and M. Shimomura, “Photo-Patterning of Honeycomb Films Prepared from Amphiphilic Copolymer Containing Photochromic Spiropyran,” *Chemical Communications* 46 (2010): 3970–3972.

26. H. Yabu, M. Takebayashi, M. Tanaka, and M. Shimomura, “Superhydrophobic and Lipophobic Properties of Self-Organized Honeycomb and Pincushion Structures,” *Langmuir* 21 (2005): 3235–3237.

27. M. Liu, X. Zhang, D. Wang, et al., “Facile Fabrication of Superhydrophobic Surface from Fluorinated Poss Acrylate Copolymer via

One-Step Breath Figure Method and its Anti-Corrosion Property," *Polymers* 11 (2019): 1953.

28. L. Li, Y. Zhong, J. Li, et al., "Thermally Stable and Solvent Resistant Honeycomb Structured Polystyrene Films via Photochemical Cross-Linking," *Journal of Materials Chemistry* 19 (2009): 7222–7227.

29. J. M. Park, Y. H. Lee, H. Park, and H. D. Kim, "Preparation and Properties of UV-Curable Fluorinated Polyurethane Acrylates," *Journal of Applied Polymer Science* 131 (2014): 40603.

30. D. Maniglio, Y. Ding, L. Wang, and C. Migliaresi, "One-Step Process to Create Porous Structures in Cross-Linked Polymer Films via Breath-Figure Formations During In Situ Cross-Linking Reactions," *Polymer* 52 (2011): 5102–5106.

31. H. Yabu, Y. Nakamichi, Y. Hirai, and M. Shimomura, "Robust Anisotropic Polymer Meshes Prepared by Stretching and Photo-Crosslinking of Poly(1,2-Butadiene) Honeycomb Films," *Physical Chemistry Chemical Physics* 13 (2011): 4877–4880.

32. W. Liu, Z. Zhou, X. Liao, et al., "Tailoring Ordered Microporous Structure of Cellulose-Based Membranes Through Molecular Hydrophobicity Design," *Carbohydrate Polymers* 229 (2020): 115425.

33. C. Carlomagno, G. Speranza, P. Aswath, G. D. Sorarú, C. Migliaresi, and D. Maniglio, "Breath Figures Decorated Silica-Based Ceramic Surfaces with Tunable Geometry from UV Cross-Linkable Polysiloxane Precursor," *Journal of the European Ceramic Society* 38 (2018): 1320–1326.

34. C. L. Casper, J. S. Stephens, N. G. Tassi, D. B. Chase, and J. F. Rabolt, "Controlling Surface Morphology of Electrospun Polystyrene Fibers: Effect of Humidity and Molecular Weight in the Electrospinning Process," *Macromolecules* 37 (2004): 573–578.

35. J. Ding, J. Gong, H. Bai, et al., "Constructing Honeycomb Micropatterns on Nonplanar Substrates with High Glass Transition Temperature Polymers," *Journal of Colloid and Interface Science* 380 (2012): 99–104.

36. H. Cong, J. Wang, B. Yu, and J. Tang, "Preparation of a Highly Permeable Ordered Porous Microfiltration Membrane of Brominated Poly(Phenylene Oxide) on an Ice Substrate by the Breath Figure Method," *Soft Matter* 8 (2012): 8835–8839.

37. C. Huang, T. Kamra, S. Chaudhary, and X. Shen, "Breath Figure Patterns Made Easy," *ACS Applied Materials and Interfaces* 6 (2014): 5971–5976.

38. J. Huang, H. Hao, Y. Huang, et al., "Gradient Porous Structure Templated by Breath Figure Method," *Langmuir* 37 (2021): 6016–6021.

39. Z. Wang, W. Guo, L. Li, et al., "Optical Virtual Imaging at 50 nm Lateral Resolution with a White-Light Nanoscope," *Nature Communications* 2 (2011): 1–6.

40. J. Kamei and H. Yabu, "One Step Fabrication of Mesh-Reinforced Hierarchic Perforated Microporous Honeycomb Films with Tunable Filtering Property," *Soft Matter* 13 (2017): 7834–7839.

41. L. Heng, X. Meng, B. Wang, and L. Jiang, "Bioinspired Design of Honeycomb Structure Interfaces with Controllable Water Adhesion," *Langmuir* 29 (2013): 9491–9498.

42. F. Galeotti, F. Trespidi, and M. Pasini, "Breath Figure-Assisted Fabrication of Nanostructured Coating on Silicon Surface and Evaluation of its Antireflection Power," *Journal of Nanomaterials* 2016 (2016): 1–8.

43. C. M. Knobler and D. Beysens, "Growth of Breath Figures on Fluid Surfaces," *Europhysics Letters* 6 (1988): 707–712.

44. P. A. Gurr, Z. Zhang, X. Hao, et al., "Highly Ordered Honeycomb Film Formation of Linear Polymers by the Breath Figure Technique," *Australian Journal of Chemistry* 69 (2016): 1130–1139.

45. E. Ferrari, P. Fabbri, and F. Pilati, "Solvent and Substrate Contributions to the Formation of Breath Figure Patterns in Polystyrene Films," *Langmuir* 27 (2011): 1874–1881.

46. H. Yamazaki, K. Ito, H. Yabu, and M. Shimomura, "Formation and Control of Line Defects Caused by Tectonics of Water Droplet Arrays During Self-Organized Honeycomb-Patterned Polymer Film Formation," *Soft Matter* 10 (2014): 2741–2747.

47. R. Daly, J. E. Sader, and J. J. Boland, "Taming Self-Organization Dynamics to Dramatically Control Porous Architectures," *ACS Nano* 10 (2016): 3087–3092.

48. A. Bolognesi, C. Mercogliano, and S. Yunus, "Self-Organization of Polystyrenes into Ordered Microstructured Films and Their Replication by Soft Lithography," *Langmuir* 21 (2005): 3480–3485.

49. F. J. Dent, D. Harbottle, N. J. Warren, and S. Khodaparast, "Exploiting Breath Figure Reversibility for In Situ Pattern Modulation," *Soft Matter* 19 (2023): 2737.

50. M. Graffiedi, F. J. Dent, S. Khodaparast, and M. Bucci, "Cryogenic Quenching Process Enhancement Through Coating and Microstructure Optimization," *Journal of Physics: Conference Series* 2766 (2024): 012139.

51. J. L. Viovy, D. Beysens, and C. M. Knobler, "Scaling Description for the Growth of Condensation Patterns on Surfaces," *Physical Review A* 37 (1988): 4965–4970.

52. H. Yabu, M. Kojima, M. Tsubouchi, S. ya Onoue, M. Sugitani, and M. Shimomura, "Fabrication of Photo-Cross Linked Honeycomb-Patterned Films," *Colloids and Surfaces A: Physicochemical and Engineering Aspects* 284-285 (2006): 254–256.

53. M. H. Chang, L. R. Lee, M. R. Huang, et al., "Light-Assisted Fabrication of Hierarchical Azopolymer Structures Using the Breath Figure Method and AAO Templates," *Langmuir* 40 (2024): 15941–15948.

54. D. H. Kim, Z. Lin, H. C. Kim, U. Jeong, and T. P. Russell, "On the Replication of Block Copolymer Templates by Poly(Dimethylsiloxane) Elastomers," *Advanced Materials* 15 (2003): 811–814.

55. C. Y. Wu, T. H. Chiang, and C. C. Hsu, "Fabrication of Microlens Array Diffuser Films with Controllable Haze Distribution by Combination of Breath Figures and Replica Molding Methods," *Optics Express* 16 (2008): 19978.

56. V. Vohra, S. Yunus, A. Attout, et al., "Bifunctional Microstructured Films and Surfaces Obtained by Soft Lithography from Breath Figure Arrays," *Soft Matter* 5 (2009): 1656–1661.

57. H. Yabu and M. Shimomura, "Simple Fabrication of Micro LLens Arrays," *Langmuir* 21 (2005): 1709–1711.

58. Y. Xia and G. M. Whitesides, "Soft Lithography," *Angewandte Chemie* 37 (1998): 550–575.

59. W. F. Quirós-Solano, N. Gaio, O. M. Stassen, et al., "Microfabricated Tuneable and Transferable Porous Pdms Membranes for Organs-On-Chips," *Scientific Reports* 8 (2018): 13524.

60. E. Mancinelli, N. Zushi, M. Takuma, et al., "Porous Polymeric Nanofilms for Recreating the Basement Membrane in an Endothelial Barrier-On-Chip," *ACS Applied Materials & Interfaces* 16, no. 10 (2024): 13006–13017.

61. C. Du, A. Zhang, H. Bai, and L. Li, "Robust Microsieves with Excellent Solvent Resistance: Cross-Linkage of Perforated Polymer Films with Honeycomb Structure," *ACS Macro Letters* 2 (2013): 27–30.

62. J. Kamei and H. Yabu, "One Step Fabrication of Mesh-Reinforced Hierarchic Perforated Microporous Honeycomb Films with Tunable Filtering Property," *Soft Matter* 13 (2017): 7834–7839.

63. T. Chen, D. Zhang, X. Tian, et al., "Highly Ordered Asymmetric Cellulose-Based Honeycomb Membrane for Moisture-Electricity Generation and Humidity Sensing," *Carbohydrate Polymers* 294 (2022): 119809.

64. C. E. Hoyle, T. Y. Lee, and T. Roper, "Thiol-Enes: Chemistry of the Past with Promise for the Future," *Journal of Polymer Science, Part A: Polymer Chemistry* 42 (2004): 5301–5338.

65. D. Sticker, R. Geczy, U. O. Häfeli, and J. P. Kutter, "Thiol-Ene Based Polymers as Versatile Materials for Microfluidic Devices for Life Sciences Applications," *ACS Appl. Mater. Interfaces* 12 (2020): 10080–10095.